ELSEVIER

Nuclear Instruments and Methods in Physics Research A 476 (2002) 522–526

NUCLEAR INSTRUMENTS & METHODS IN PHYSICS RESEARCH Section A

www.elsevier.com/locate/nima

A gamma-ray spectrometer system for fusion applications

B. Esposito[a,*], L. Bertalot[a], Yu.A. Kaschuck[b], D.V. Portnov[b], J.R. Martin-Solis[c]

[a] *Associazione Euratom-ENEA sulla Fusione, C.R. Frascati, C.P. 65, I-00044 Frascati, Roma, Italy*

[b] *TRINITI, Troitsk, Moscow Region 142092, Russia*

[c] *Universidad Carlos III de Madrid, Avenida de la Universidad 30, Leganes, 28911-Madrid, Spain*

Abstract

A NaI scintillator spectrometer system for the measurement of gamma-ray spectra in tokamak discharges has been developed and installed on the Frascati Tokamak Upgrade. Two NaI scintillators are viewing the plasma at two different angles with respect to the equatorial plane. The main features of the spectrometer system (energy range: 0.3–23 MeV) and of the unfolding technique used to restore physical spectra from the pulse-height distributions are described: a method of solution with regularisation for matrix equations of large size, allowing to process count distributions with significant statistical noise, has been developed. A dedicated software, portable to any platform, has been written both for the acquisition and the analysis of the spectra. The typical gamma-ray spectra recorded in hydrogen and deuterium discharges, also with additional heating, are presented and discussed; two components have been observed: (a) thick-target bremsstrahlung gamma-rays produced by runaway electrons hitting the inconel poloidal limiter and/or the vessel; and (b) neutron capture gamma-rays generated in the detector shielding and tokamak structures. The maximum energy resulting from the bremsstrahlung spectra is in agreement with the runaway energy predicted by a test particle model of runaway electron dynamics.

1. Introduction

The measurement of the gamma-ray spectra produced in the Frascati Tokamak Upgrade (FTU) machine represents a useful tool to study the dynamics of runaway electrons in a tokamak plasma. Other fusion related issues concerning runaways are the mechanisms of runaway generation in plasma disruptions [1] and the study of magnetic turbulence [2]. Gamma-rays are emitted, via thick-target bremsstrahlung, when runaway electrons are lost from the plasma and hit the inconel limiter or the vessel structures. Such gamma-ray emission is detected in a mixed neutron/gamma field, whose main components are: (a) thermonuclear fusion D–D neutrons and D–T neutrons (tritium results as a by-product from D–D reactions); (b) gamma-rays produced by thick-target bremsstrahlung of runaway electrons; (c) gamma-rays from neutron capture reactions; and (d) photoneutrons produced by gamma radiation. Two NaI gamma-ray spectrometers have been installed on FTU, each one providing 16 spectra per discharge. Additional information on the neutron/gamma production is yielded by a system of calibrated BF_3 proportional chambers (located in pairs, 120° apart, above the torus [3]) and a $5'' \times 5''$ NE213 scintillator.

*Corresponding author. Tel.: +39-06-9400-5152; fax: +39-06-9400-5400.

E-mail address: esposito@frascati.enea.it (B. Esposito).

0168-9002/02/$ - see front matter
PII: S0168-9002(01)01501-7

2. Experimental set-up and spectrum unfolding technique

The gamma-ray spectrometers are two identical $3'' \times 3''$ NaI scintillators, which permit to use standard methods of response function calculations and spectra unfolding [4]. The detectors are placed at the same toroidal position (the angle between the detectors and the poloidal limiter being $\sim 150^\circ$) but in different poloidal locations (0° and $\sim 50^\circ$, respectively, for detectors #1 and #2). The detector on the equatorial plane (#1) is shielded using layers of various materials (polyethylene, lead), and its collimator ($\sim 7 \times 2$ cm wide and 15 cm long) looks at the plasma/limiter and has a wide field of view ($\sim 26^\circ$). The detector #2 is only shielded with lead bricks (~ 25 cm thick) and has no front collimator. Both spectrometers are located outside the machine cryostat and therefore detect photons which have traversed various radiation-absorbing materials (e.g. coils, vessel). The energy range for both detectors is set to ~ 0.3–23 MeV with 1024 channel resolution; the energy calibration has been performed in the low-energy range (up to 3 MeV) by means of standard radioactive sources and extended linearly up to higher energy. Both detectors can operate correctly up to 100 kHz; for higher count rates (usually in plasma disruptions) saturation effects take place with consequent strong spectral distortion. The acquisition system is based on CAMAC modules; hardware timing is used to obtain good precision in the 16 programmable time windows (one every 0.1 s) in each plasma discharge. A dedicated software package for data acquisition, analysis and visualization has been developed in the graphical programming G language (LabVIEW environment[1] [5]), which allows full portability to any platform. The system, controlled by a Macintosh personal computer (on which the acquired data are stored) via a CAMAC-GPIB interface, has been designed to be stand-alone, requiring, apart from the input signal, only the external trigger to start the acquisition, and can therefore be quickly installed on any other experimental facility. Moreover, by means of an Ethernet GPIB controller (GPIB-ENET module [5]) the CAMAC modules are operated remotely via Ethernet.

The software also includes a spectrum unfolding algorithm; the problem of restoring the physical spectrum from the measured pulse height distribution can be represented by the following integral equation:

$$\Phi(p) = \int_0^{E_{\max}} k(E,p)\Psi(E)\,\mathrm{d}E \tag{1}$$

where E is the energy of the photon, p the photon energy deposited in the scintillator (pulse height), $\Psi(E)$ the density of energy distribution of photons and $k(E,p)$ the response function of the detector (probability to obtain the deposited energy p if the incoming photon has energy E). The goal of the unfolding procedure is to compute the energy distribution $\Psi(E)$ from a given pulse height distribution $\Phi(p)$ and response function $k \times (E,p)$. In practice Eq. (1) can be rewritten as a matrix equation

$$A\Psi = \Phi \tag{2}$$

where A is the folding matrix, Φ the measured pulse height distribution and Ψ the unknown spectrum. A direct solution of Eq. (2) is only possible in case of very smooth and monotonic distributions with absolutely no noise; even a very low amount of noise in the matrix Φ (corresponding to the experimental data) results in an unacceptable noise in the solution. In order to properly handle the noise in the experimental data, a regularized solution of Eq. (2) is obtained by using the condition that the distribution Ψ_i, to a certain extent, is continuous and smooth; this means $(\Psi_{j+1} - \Psi_j)/(E_{j+1} - E_j) \cong (\Psi_j - \Psi_{j-1})/(E_j - E_{j-1})$. Therefore, instead of a direct solution from the minimization of $|A\Psi - \Phi|$, we look for a solution which minimizes $|A\Psi - \Phi| + \alpha|u|$, where α is a regularizing parameter, $u = D\Psi$ and D a tridiagonal matrix with elements $D_{j,j-1} = (E_{j+1} - E_j)/(E_{j+1} - E_{j-1})$; $D_{j,j} = -1$; $D_{j,j+1} = (E_j - E_{j-1})/(E_{j+1} - E_{j-1})$, where $j = 2, \ldots, N-1$ and the first and last rows are set to zero. It can be shown that Ψ is a

[1] LabVIEW is a trademark of National Instruments Corporation.

solution of

$$K\Psi = R \tag{3}$$

where $K = A^{\mathrm{T}}A + \alpha D^{\mathrm{T}}D$ and $R = A^{T}\Phi$. The regularization parameter α is then selected empirically, according to test estimates. Eq. (3) can be solved with standard Cholesky decomposition [6], provided that K is symmetric. The unfolding software has been originally written in C++ with a 256×256 matrix; however, for fast analysis and display of the unfolded spectra, it has also been implemented (with a reduced size 77×77 matrix) in the LabVIEW spectrometric system program. Weights representing the statistical significance of the measurement Φ can also be simply included in the unfolding procedure. A typical test case is shown in Fig. 1, where a non-monotonic type of spectrum with a high level of noise (calculated using a binomial distribution) is used: the 4 curves represent the original spectrum (Gaussian curve), the folded spectrum with noise, the unfolded spectrum and its refolded spectrum. The response matrix was calculated for non-uniform binning corresponding to ~ 3 bin per FWHM of expected energy resolution at the corresponding energy.

The main advantage of the present unfolding method, compared with similar methods such as FERD [7], is the fact that the regularizing term does not depend on the experimental data Φ. Therefore, it is not necessary to recalculate the final conditioned matrix K for every distribution Φ (as in FERD), but the matrix K is calculated only once for given matrix A and regularizing parameter α (and, if used, weight matrices) and can be used for any given Φ distribution.

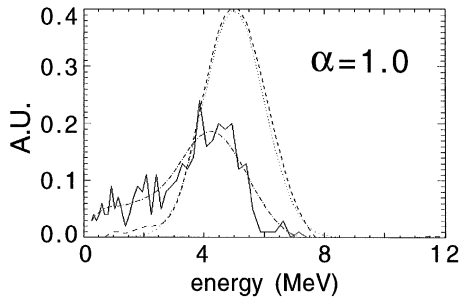

Fig. 1. Unfolding test: initial Gaussian spectrum (dotted); folded spectrum + noise (solid); unfolded spectrum (dashed); folding of unfolded spectrum (dot-dashed).

3. Experimental results

Two different components are present in the measured FTU gamma-ray spectra: (a) gamma-rays from thick-target bremsstrahlung of runaway electrons and (b) gamma-rays from neutron capture reactions. Typical pulse height spectra of these two components are compared in Fig. 2; the runaway thick-target bremsstrahlung spectrum is obtained from a hydrogen discharge (#16362) and the neutron capture spectrum from a runaway-free high density deuterium discharge (#15443; the unfolded spectrum is also shown). The neutron capture component, which is proportional to the neutron emission, constitutes a background in all discharges (except for the hydrogen ones where it is practically absent) and the shape of this spectrum is fixed with a maximum energy of ~ 10 MeV; on the contrary, the bremsstrahlung component only appears when runaway electrons are present and the spectrum shape varies depending on the energy and distribution function of the

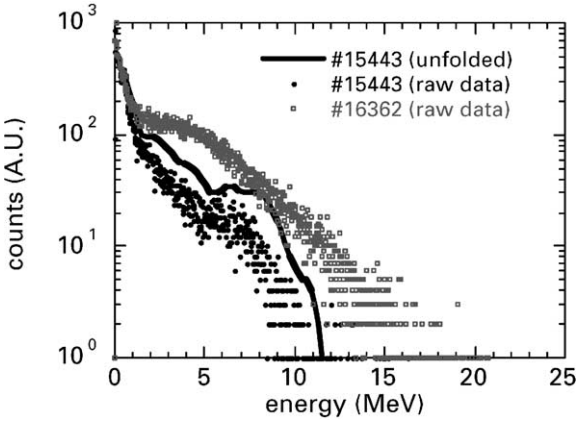

Fig. 2. Comparison between pulse height distributions of bremsstrahlung gamma-rays due to runaway electrons (#16362) and gamma-rays from neutron capture (#15443); unfolded spectrum for #15443 is also shown.

runaway electron beam: the measured maximum gamma energy is ~ 20 MeV. In deuterium discharges, the presence of runaways is also evidentiated by a comparison between the time traces of the neutron detectors: the NE213 detector, sensitive to both neutrons and gamma-rays, has been cross-calibrated with the BF_3 chambers (only sensitive to neutrons) in selected high-density discharges with negligible runaway production; when the time traces of the NE213 scintillator and the BF_3 chambers do not overlay but the NE213 signal exceeds the one BF_3 signal, runaway electrons are present (see Fig. 3).

The spectrometer #2 correctly measures the same neutron capture gamma-ray background as detector #1. However, when runaways are present detector #2 produces spectra with apparently different slopes. As an example, in Fig. 4 are plotted the spectra obtained from the two spectrometers at different times in a runaway hydrogen discharge (#16803): in the ohmic phase, $t = (0-1)$ s, the slopes of the spectra from detectors #1 and #2 are different (the gamma maximum energy, from the end point of the gamma pulse height distribution, is ~ 20 MeV); during the auxiliary heating phase with lower hybrid, $t = (1.0-1.4)$ s, the measured maximum gamma energy is much lower (~ 1–2 MeV) and the two spectra have a similar slope. For this discharge, a rough estimate of the runaway electron current loss can also be inferred by combining information from the gamma spectrometers and the neutron detectors (see the time trace in Fig. 5); it is clearly seen that the neutrons, which are present during the ohmic phase, disappear during LH when the measured gamma energy goes below the threshold for photonuclear reactions [8]. Therefore, the observed neutrons during the ohmic phase ($N_{NEU} \sim 2 \times 10^9\ s^{-1}$) can be assumed to be due to photonuclear reactions occurring when runaways

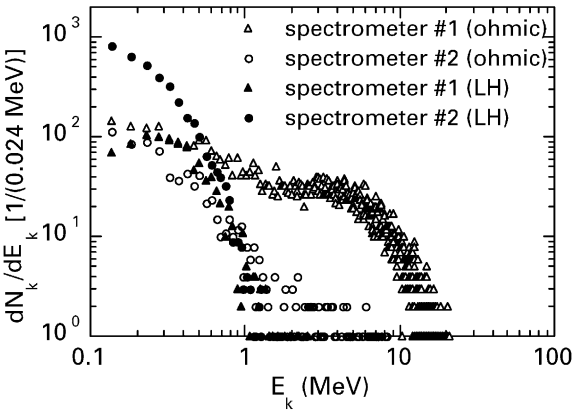

Fig. 4. Pulse height distributions from both spectrometers during the ohmic and LH phases of a hydrogen discharge (#16803).

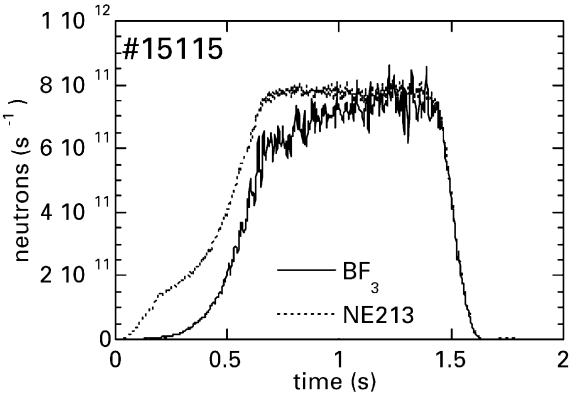

Fig. 3. Time traces of BF_3 chambers and NE213 scintillator during a deuterium discharge with presence of runaways for $t < 1.2$ s.

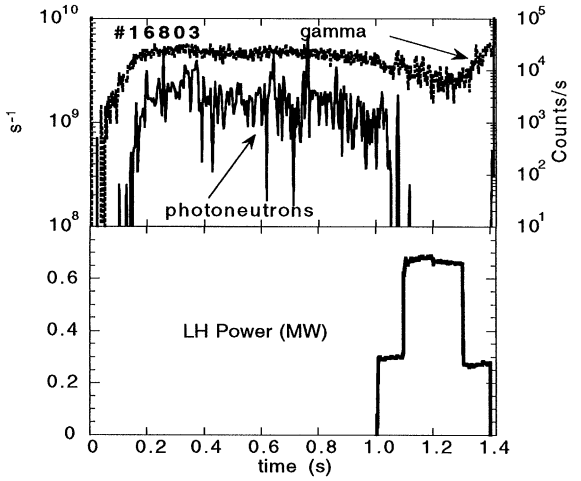

Fig. 5. Gamma-ray spectrometer integral counts, neutrons and LH additional power (lower trace) vs. time in discharge #16803.

hit the limiter and/or the vessel. The production of photoneutrons is mainly localized in the poloidal limiter as indicated by a toroidal asymmetry in the measured neutron emission (i.e. higher counts from the BF_3 detectors placed close to the limiter). As the energy of the runaways is roughly 20 MeV, the photoneutron yield/electron ratio $Y \sim 5 \times 10^{-4}$–10^{-3} [9] and the total runaway electron loss is given by $N_R = N_{NEU}/Y \sim 4 \times 10^{12}\,s^{-1}$.

4. Estimate of runaway electron energy

The subtraction from the measured spectrum of the neutron capture gamma-ray component (normalized to the actual neutron emission in each time window as determined by the BF_3 chambers) has been performed in the case of deuterium discharges in order to extract the gamma-ray component due to the runaway electrons: the neutron capture gamma-ray spectrum used as a reference is taken from a runaway free discharge. The measured runaway maximum energy, assumed to correspond to the end point of the gamma pulse height distribution, has been compared with the prediction of a test particle model of runaway dynamics [10] which includes acceleration in the electric field, collisions with the plasma particles and synchrotron radiation losses. The results for discharge #16803 are shown in Fig. 6: the solid line corresponds to the simulation performed using $E_R = 1$ MeV as initial energy of the electron at $t = 0.1$ s. The agreement between model and experimental data indicates that the runaway dynamics in these discharges is strongly sensitive to the toroidal electric field and the plasma density [8].

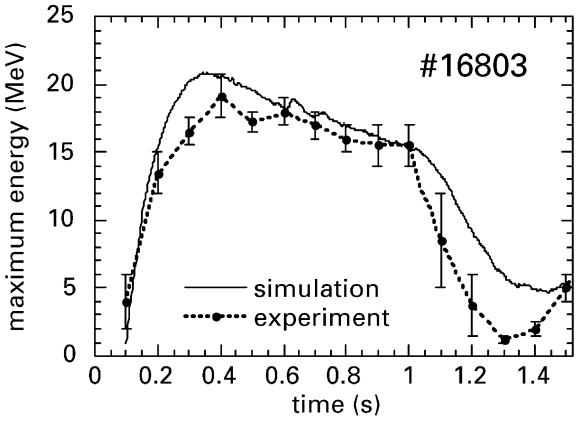

Fig. 6. Runaway electron maximum energy: comparison between experiment and theory.

References

[1] R.D. Gill, B. Alper, A.W. Edwards, et al., Nucl. Fusion 40 (2000) 163.
[2] I. Entrop, N.J. Lopes-Cardoso, R. Jaspers, K.H. Finken, Phys. Rev. Lett. 84 (2000) 3606.
[3] M. Angelone, P. Batistoni, L. Bertalot, et al., Rev. Sci. Instr. 61 (1990) 3536.
[4] M.J. Berger, S.M. Seltzer, Nucl. Instr. and Meth. 104 (1972) 317.
[5] http://www.ni.com
[6] J.H. Wilkinson, C. Reinsch, in: Linear Algebra Handbook for Automatic Computation, Vol. II, Springer, New York, 1971.(Chapter I/1)
[7] W.R. Burrus, ORNL-3743 Report, 1965;
B.W. Rust, W.R Burrus, DASA 2604 Report, 1972.
[8] J.R. Martin-Solis, B. Esposito, R. Sanchez, et al., Proceedings of the 27th EPS Conference on Plasma Physics and Controlled Fusion, Budapest, 2000.
[9] G. Maddaluno, B. Esposito, J. Nucl. Mater. 266–269 (1999) 593.
[10] J.R. Martin-Solis, et al., Phys. Plasmas 5 (1998) 2370.